Optics Letters

Visible upconversion luminescence of doped bulk silicon for a multimodal wafer metrology

Boris I. Afinogenov,[1,2] Anton N. Sofronov,[1,*] Ilya M. Antropov,[2] Nikita R. Filatov,[2] Anton S. Medvedev,[1] Alexander S. Shorokhov,[1,2] Vladimir N. Mantsevich,[2] Natalia S. Maslova,[2] Taehyun Kim,[3] Eunhee Jeang,[3] Ingi Kim,[3] Minhwan Seo,[3] Kyunghun Han,[3] Sangwoo Bae,[3] Wondon Joo,[3] Hosun Yoo,[3] Vladimir O. Bessonov,[2] Andrey A. Fedyanin,[2] Maksim V. Ryabko,[1] and Stanislav V. Polonsky[1]

[1]Samsung R&D Institute Russia, Moscow 127018, Russia
[2]Faculty of Physics, Lomonosov Moscow State University, Moscow 119991, Russia
[3]Core Technology R&D Team, Mechatronics R&D Center, Samsung Electronics, Hwaseong-si, Republic of Korea
*Corresponding author: a.sofronov@samsung.com

Received 11 March 2021; accepted 24 May 2021; posted 1 June 2021 (Doc. ID 424834); published 21 June 2021

We report the experimental observation of the UV-visible upconverted luminescence of bulk silicon under pulsed infrared excitation. We demonstrate that non-stationary distribution of excited carriers leads to the emission at spectral bands never to our knowledge observed before. We show that the doping type and concentration alter the shape of luminescence spectra. Silicon nanoparticles have a size between quantum-confined and Mie-type limits (10–100 nm) yet show increased luminescence intensity when placed atop a silicon wafer. The findings demonstrate that upconversion luminescence can become a powerful tool for nearest future silicon wafer inspection systems as a multimodal technique of measuring the several parameters of the wafer simultaneously. © 2021 Optical Society of America

https://doi.org/10.1364/OL.424834

A demand for faster and higher-resolution inspection tools pushes technology beyond the current limits. Conventional techniques are either resolution-limited like dark-field microscopy [1], slow like scanning tunneling microscopy [2], or destructive like scanning electron microscopy combined with the ion-beam cuts. An ideal novel method should be multimodal: allowing for simultaneous dopant density profiling, defectoscopy, strain/stress mapping, and characterization of a wafer by other parameters [3]. Promising candidates for that are nonlinear-optics techniques including Raman or frequency-conversion microscopies [4–7]. Luminescence microscopy is another tool that is widely used for characterizing semiconductor wafers and devices [8].

Despite the low efficiency of silicon optical response, conventional photoluminescence (PL) in spectral range around the bandgap $E_g \approx 1.1$ eV [9,10] from thermalized carriers [11] is extensively studied for coarse mapping of dopant density across silicon wafers in photovoltaic devices [12,13]. Hot-carriers luminescence was observed in bulk silicon $p-n$ junctions under conditions of the constant electric injection of high-energy electrons [14–17]. Alternatively, hot carriers can be generated by strongly localized excitation light inside silicon mediated by plasmonic [18–20] resonances, when the optical response is enhanced by the increase in the photonic density of states.

Specific emission from silicon nanoparticles (NPs) is observed in two extreme cases. The first one requires quantum confinement and occurs in quantum dots—particles smaller than 10 nm [21]. In this case, modification of electronic density of states relaxes the k-conservation rule resulting in bright UV-visible emission [22]. The second case realizes when silicon NPs are larger than 150 nm and support Mie resonances [23]. In this extreme, UV-visible emission is mediated by hot carriers generated by a strongly localized pump field.

Surprisingly, there is no study, to the best of our knowledge, that addresses luminescent properties of pristine bulk silicon in visible range. Moreover, emission from NPs whose size is between quantum limit and Mie limit has not been explored as well. Here, we report the observation of a broadband upconverted UV-visible PL from bulk silicon under femtosecond near-infrared (IR) excitation. We show that PL spectrum has multiple peaks that appear only in the non-stationary excitation regime with spectral positions depending on the doping level. We demonstrate that silicon NPs that do not possess geometric resonances enhance PL efficiency. Finally, we discuss how this novel phenomenon can be employed in the next-generation metrology tools.

We study four samples of silicon wafers: one n-type with a doping level of 10^{15} cm^{-3} (n-15) and three p-type with doping levels of 10^{15} cm^{-3} (p-15), 10^{18} cm^{-3} (p-18), and 10^{20} cm^{-3} (p-20). Cylindrical NPs with a height of 20 nm and diameters ranging from 20 nm to 200 nm are prepared on the p-18 wafer.

We measure PL spectra with a custom microscope spectrometer (see Methods in Supplement 1) using a 150 fs Ti:sapphire laser as an excitation source. The central wavelength of the

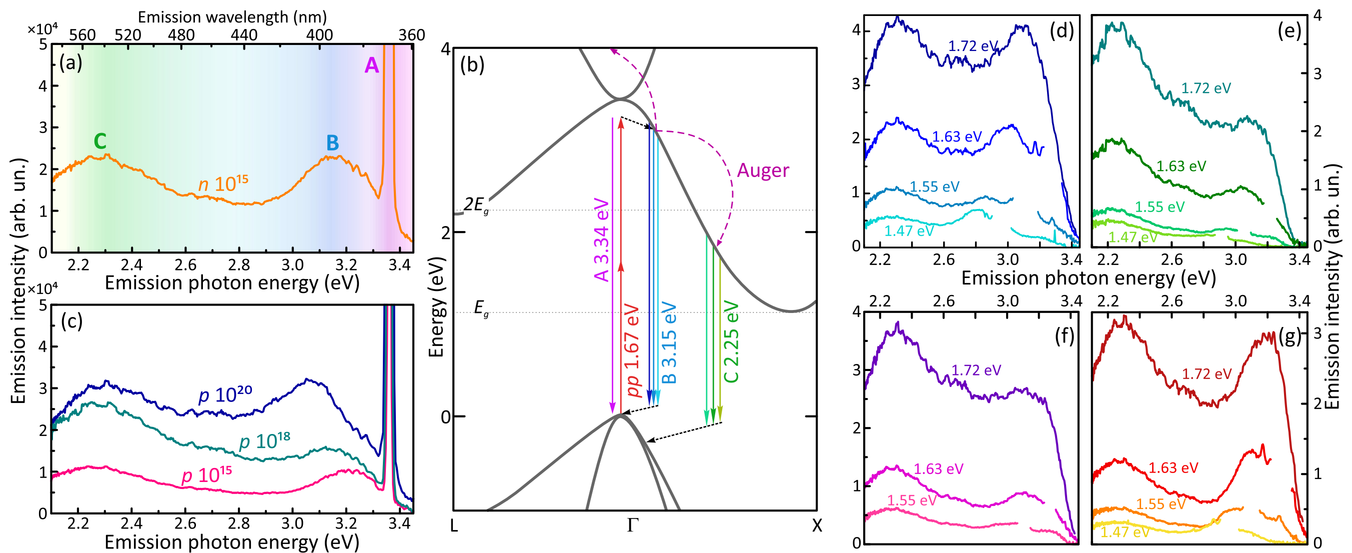

Fig. 1. (a) Luminescence spectrum of n-doped bulk silicon. Pump photon energy is 1.67 eV. (b) Schematic bandstructure of silicon and electronic transitions responsible for absorption and emission. (c) Luminescence spectra of p-type doped bulk silicon. Pump photon energy is 1.67 eV. (d)–(g) Luminescence spectra depending on the pump photon energy for (d) p-20, (e) p-18, (f) p-15, and (g) n-15 samples. Second-harmonic peaks are omitted for clarity. Average fundamental power is 50 mW.

fundamental radiation is tunable in range 700–840 nm (pump photon energy $\hbar\omega_{pp}$ 1.77–1.47 eV).

Figure 1(a) shows emission spectrum of the n-15 wafer under $\hbar\omega_{pp} = 1.67 - \text{eV}$ with the corresponding electronic transitions shown in Fig. 1(b). Average pump power is 50 mW. Three main features [labeled as A, B, and C in Fig. 1(a)] are clearly distinguished. A sharp resonance A at 3.35 eV corresponds to the second-harmonic generation [24]. Broader peaks B and C are associated with emission from hot electrons. However, we suggest that their origin is markedly different.

An intense femtosecond laser pulse creates strongly athermal distribution of electrons determined by one- and multiphoton absorption processes. At intensities in the order of 10^{11} W/cm^2 used in experiment, the coefficient of two-photon absorption is comparable with the linear absorption coefficient while higher-order absorption can still be neglected [25]. Thus, the initial hot-electron distribution in the conduction band (CB) spans from 0 (the bottom of the band) to $2\hbar\omega_{pp} - E_g$. Moreover, the top of the valence band (VB) becomes strongly depleted.

During thermalization, part of two-photon excited electrons experience immediate radiative transitions back to the depleted levels around top of the VB. Peak B spectrally located close to the $2\hbar\omega_{pp}$ energy is assumed to be caused by this process. The spectral detuning between peaks A and B is defined by twice the energy of a phonon, required for an indirect transition. This peak is a signature of the ultrashort-pulse IR excitation used in experiment. Constant electronic injection or c.w.-optical pumping does not create distribution of electrons, which allows the observed transitions. As the thermalization time is in the order of tens-to-hundreds of femtoseconds, the time scale of the emission responsible for peak B should be rather fast.

We associate origin of the peak C with the intraband Auger processes, which occur due to the strong Coulomb interaction between excited carriers. Electron–electron interaction lifts one of the carriers from initial states around $2\hbar\omega_{pp}$ to high-energy states due to the Auger effect with the following non-radiative relaxation. At the same time, another carrier scatters to the low-energy states and further contributes to the PL in the peak C band. The full theoretical model describing formation of the peak C is given in Supplement 1.

PL spectra for p-type doped silicon are shown in Fig. 1(c). Silicon wafers with p-type doping have less doping-related lattice defects as compared with n-type doped wafers [26]. A larger number of lattice defects creates an additional electron scattering channel and results in the increased probability of indirect transitions responsible for the PL. Thus, the p-15 sample shows the lower PL intensity when compared with n-15 sample. With the increase of the p-type doping level, the overall intensity of PL grows. This is defined in part by the higher absorption of more heavily doped silicon [27]. Another factor is the decrease of the radiative lifetime of the excited carriers due to higher probability of scattering at dopant impurities. Remarkably, peak B experiences a pronounced redshift for about 200 meV with the increase of the doping concentration from 10^{15} cm^{-3} to 10^{20} cm^{-3}. It was reported [28] that relaxation time of carriers decreases at higher doping levels. As we attribute peak B to the fast emission from the non-thermalized carriers, smaller relaxation time eventually leads to the larger excess energy loss before emission.

Upon redshift of the pump wavelength, the PL intensity decreases following the behavior of absorption. Figures 1(d)–1(g) show luminescence spectra for all samples illuminated at four different excitation wavelengths with the intensity kept at the same level. Second-harmonic peak positions strictly follow $2\hbar\omega_{pp}$ law and are omitted for clarity. Besides overall-reduced PL intensity, we observe that peaks B and C behave differently when the energy of the pump photon decreases. Peak C nearly does not change its spectral position around 2.25 eV, which serves as an additional proof that the peak is related to the silicon bandstructure. In contrast, peak B redshifts with the excitation wavelength since it is caused by instantaneous emission of two-photon excited electrons. The decrease of

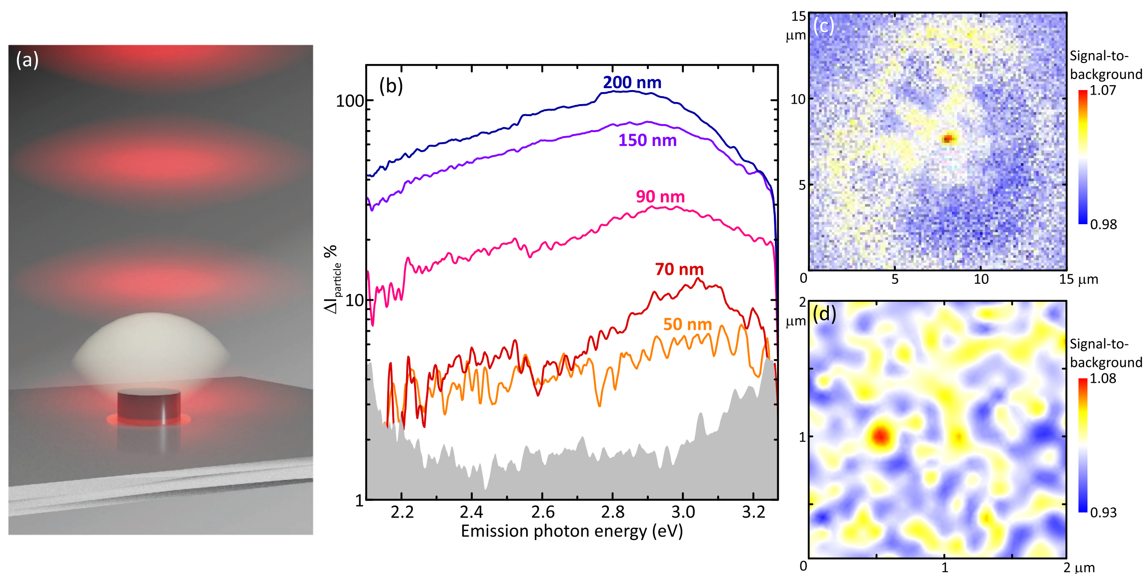

Fig. 2. (a) Sketch of the nanoparticle-mediated enhancement of silicon luminescence. (b) Spectra of the luminescence enhancement caused by nanoparticle for different particle sizes. Gray area represents the measured uncertainty of the luminescence intensity from a bare Si wafer. (c) Nonlinear-luminescence image of the 60 nm Si nanoparticle atop the Si wafer obtained in a Köhler illumination regime. (d) Nonlinear-luminescence image of the 40 nm Si nanoparticle obtained in the scanning illumination regime. Pump photon energy in (b)–(d) is 1.67 eV.

spectral distance between peak B and $2\hbar\omega_{pp}$ observed with the redshift of the pump photon energy is expected as well since the thermalization time is usually higher for lower energy electrons. The relative intensity of peaks B and C is changed upon tuning the pump wavelength. As the reduced absorption results in the smaller amount of the excited carriers, this phenomenon can be caused by the different exponents in the dependence of emission intensity on the electron density. We measure the PL spectra at different pump powers and observe a complicated behavior since the exponent of the emission intensity on the pump power is determined by a number of factors analyzed in Supplement 1.

Figure 2(b) shows spectra of the relative PL enhancement collected from the area with NP as compared with a pristine silicon surface. The illuminated area is defined by the diffraction-limited spot of approximately 950 nm in diameter, and only one NP is present in this area at a time. The total additional luminescence intensity caused by a NP varies from 100% for a 200 nm NP to 5% for a 50 nm NP. The gray area in Fig. 2(b) shows the uncertainty of the luminescence intensity from a bare Si wafer obtained as a standard deviation over 10 spectra measured at different points of the wafer.

We performed FDTD calculations (shown in Supplement 1) to check the fundamental field enhancement factor depending on the NP size. Indeed, for the 200 nm NP, the pump field inside the wafer is enhanced up to the factor of 1.35 as compared with a clean surface. For the largest particle, the pump field localization gives rise to additional 64% luminescence in an average over emission range. For the 40 nm NP, the localization-related addition to the luminescence is 2%. Thus, weak localization of the pump field inside silicon is responsible for the upconversion PL enhancement in our experiments.

Even the minor increase of the PL intensity by small NPs allows for their reliable imaging using nonlinear-optical methods. Figures 2(c)–2(d) show images of the 60 nm and 40 nm

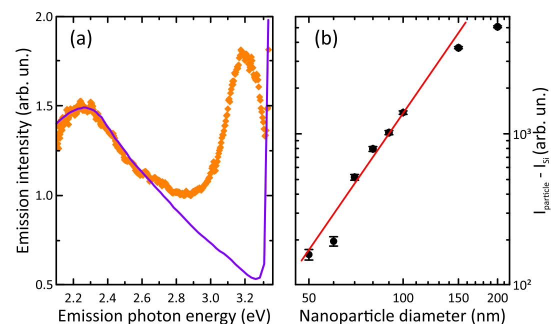

Fig. 3. (a) Experimental (dots) and theoretical (solid line) luminescence spectra of n-doped bulk silicon. Pump photon energy is 1.67 eV. (b) Log-log plot of an additional luminescence signal caused by a nanoparticle integrated over emission range versus size of a nanoparticle. Solid line shows a cubic power-law.

NPs obtained under Köhler and focused-spot-scanning illuminations (see Methods in Supplement 1), respectively. Köhler illumination allows for imaging the larger area on the wafer. However, the particle visualization is limited by the inhomogeneities of the fundamental beam. The focused-illumination imaging in turn is limited by the wafer unevenness and allows for the detection of smaller NPs.

The full derivation of equations describing the Auger-related PL is given in Supplement 1. Figure 3(a) shows a measured spectrum of the luminescence of an n-15 sample along with the one calculated from a theoretical model. It can be seen that the theoretical curve fits both peaks A [only low-energy slope of the peak is shown in Fig. 3(a)] and C, which serves as a proof of the proposed description.

Luminescence intensity is a sum of contributions from a bulk of silicon and silicon NP S_{NP}:

$$S_{\mathrm{NP}}(\hbar\omega_e) \propto \frac{d^3}{R^3}\overline{L^4(d)}, \quad (1)$$

where L is a local field factor, d is a NP size, and R^3 corresponds to the volume by which the measured signal is averaged. For the small NPs, $d < \lambda$ the averaged local field factor $\overline{L^4(d)}$ nearly does not depend on d. Thus, the additional PL intensity should scale as d^3. Figure 3(b) shows the additional PL intensity integrated over emission range versus the size of a NP along with the cubic power-law fit. Indeed, the $\Delta I \propto d^3$ law holds for NPs smaller than 100 nm, while for larger NPs local field factor starts playing an important role.

The upconversion luminescence can be put into practice for the multimodal silicon metrology tool. First, the dopant density alters the intensity of the luminescence peak C and leads to the pronounced spectral shift of the peak B. Since we use near-IR light as pump radiation, PL is generated in a thick slab of a wafer. However, intrinsic absorption of silicon governs the spectral profile of the emission depending on the depth of the emission region. Accordingly, emission responsible for peak C contains information from deep-lying regions of a wafer, while peak B corresponds to the emission from shallow regions close to the surface of a wafer. Second, silicon NPs atop the wafer enhance PL intensity, which allows for their reliable detection. Moreover, additional luminescence caused by NP scales with its size as d^3. This is a significant advantage over currently used dark-field techniques, which detect scattered signal scaling as d^6. Spectral band of the most significant NP-induced PL enhancement is located between peaks B and C. Thus, tri-band hyperspectral imaging allows for simultaneous identification of NPs and dopant density mapping.

NPs of other materials placed on the silicon wafer will have different influence on upconversion PL intensity and spectral profile. Metal NPs strongly localize the pump field in the wafer, and the spectral dependence of enhancement will be governed by plasmonic resonances of NPs. Dielectric NPs will most likely cause weaker but spectrally even increase of PL intensity. This allows for another modality of the technique, namely classification of NPs by material. Upconversion luminescence can be easily utilized to study samples protected with oxide layers and patterned wafers. Azimuthal dependence of the PL intensity allows us to consider that the technique will be sensitive to the local symmetry breaking due to stress/strain in a wafer.

In conclusion, we experimentally demonstrated the visible upconverted luminescence of bulk silicon under femtosecond IR excitation. We performed a systematic study of the modification of the PL intensity by doping type and density and the presence of the NPs atop the surface. The presence of the luminescence should be taken into account in the spectroscopic or imaging studies of silicon devices as it may create a uniform parasitic background. The phenomenon is useful for the next-generation inspection and characterization of silicon wafers including dopant density mapping and repeatable detection of nanodefects on wafers. Elucidating mechanisms responsible for the UV-visible luminescence in bulk silicon is important for the development of the novel CMOS-compatible light emitters.

Acknowledgment. I. M. A, V. O. B., and A. A. F acknowledge support by the Development Program of the Interdisciplinary Scientific and Educational School of Lomonosov Moscow State University "Photonic and Quantum technologies. Digital medicine."

Disclosures. The authors declare no conflicts of interest.

Data Availability. Data underlying the results presented in this paper are not publicly available at this time but may be obtained from the authors upon reasonable request.

Supplemental document. See Supplement 1 for supporting content.

REFERENCES

1. S. Cho, J. Lee, H. Kim, S. Lee, A. Ohkubo, J. Lee, T. Kim, S. Bae, and W. Joo, Opt. Lett. **43**, 5701 (2018).
2. M. Usman, J. Bocquel, J. Salfi, B. Voisin, A. Tankasala, R. Rahman, M. Y. Simmons, S. Rogge, and L. Hollenberg, Nat. Nanotechnol. **11**, 763 (2016).
3. N. G. Orji, M. Badaroglu, B. M. Barnes, C. Beitia, B. D. Bunday, U. Celano, R. J. Kline, M. Neisser, Y. Obeng, and A. Vladar, Nat. Electron. **1**, 532 (2018).
4. T. Kunz, M. T. Hessmann, S. Seren, B. Meidel, B. Terheiden, and C. J. Brabec, J. Appl. Phys. **113**, 023514 (2013).
5. J. L. Fiore, V. V. Fomenko, D. Bodlaki, and E. Borguet, Appl. Phys. Lett. **98**, 041905 (2011).
6. M. L. Alles, R. Pasternak, X. Lu, N. H. Tolk, R. D. Schrimpf, D. M. Fleetwood, R. P. Dolan, and R. W. Standley, IEEE Trans. Semicond. Manuf. **20**, 107 (2007).
7. O. Aktsipetrov, A. Fedyanin, E. Mishina, A. Rubtsov, C. Van Hasselt, M. Devillers, and T. Rasing, Phys. Rev. B **54**, 1825 (1996).
8. S. Perkowitz, *Optical Characterization of Semiconductors: Infrared, Raman, and Photoluminescence Spectroscopy* (Elsevier, 2012).
9. J. Haynes and W. Westphal, Phys. Rev. **101**, 1676 (1956).
10. G. Davies, Phys. Rep. **176**, 83 (1989).
11. A. Sabbah and D. M. Riffe, Phys. Rev. B **66**, 165217 (2002).
12. T. Trupke, R. Bardos, M. Schubert, and W. Warta, Appl. Phys. Lett. **89**, 044107 (2006).
13. T. Trupke, J. Nyhus, and J. Haunschild, Phys. Status Solidi RRL **5**, 131 (2011).
14. P. Schmidt, R. Berndt, and M. I. Vexler, Phys. Rev. Lett. **99**, 246103 (2007).
15. L. Snyman, M. Du Plessis, E. Seevinck, and H. Aharoni, IEEE Electron Device Lett. **20**, 614 (1999).
16. M. A. Green, J. Zhao, A. Wang, P. J. Reece, and M. Gal, Nature **412**, 805 (2001).
17. L. W. Snyman, M. Du Plessis, and E. Bellotti, IEEE J. Quantum Electron. **46**, 906 (2010).
18. C.-H. Cho, C. O. Aspetti, J. Park, and R. Agarwal, Nat. Photon. **7**, 285 (2013).
19. C. O. Aspetti, C.-H. Cho, R. Agarwal, and R. Agarwal, Nano Lett. **14**, 5413 (2014).
20. Z. Mu, H. Yu, M. Zhang, A. Wu, G. Qi, P. K. Chu, Z. An, Z. Di, and X. Wang, Nano Lett. **17**, 1552 (2017).
21. W. L. Wilson, P. Szajowski, and L. Brus, Science **262**, 1242 (1993).
22. Q. Li, T.-Y. Luo, M. Zhou, H. Abroshan, J. Huang, H. J. Kim, N. L. Rosi, Z. Shao, and R. Jin, ACS Nano **10**, 8385 (2016).
23. C. Zhang, Y. Xu, J. Liu, J. Li, J. Xiang, H. Li, J. Li, Q. Dai, S. Lan, and A. E. Miroshnichenko, Nat. Commun. **9**, 1 (2018).
24. O. A. Aktsipetrov, I. Baranova, and K. Evtyukhov, *Second Order Non-linear Optics of Silicon and Silicon Nanostructures* (CRC Press, 2018).
25. D. S. Polyakov and E. B. Yakovlev, Opt. Quantum Electron. **50**, 235 (2018).
26. R. J. Van Overstraeten and R. P. Mertens, Solid State Electron. **30**, 1077 (1987).
27. G. Jellison, Jr., S. Withrow, J. McCamy, J. Budai, D. Lubben, and M. Godbole, Phys. Rev. B **52**, 14607 (1995).
28. A. Borghesi, P. Bottazzi, G. Guizzetti, L. Nosenzo, A. Stella, S. Campisano, E. Rimini, F. Cembali, and M. Servidori, Phys. Rev. B **36**, 9563 (1987).